Machining Tool and Bearing Failure Analysis Using the Orthogonal Hilbert-Huang Transform on Vibration and Motor Current Datasets

Trent S. Furlong[1], Dr. Karl M. Reichard[2]

[1,2]*The Pennsylvania State University, State College, PA, 16801, United States*

tsf44@psu.edu
kmr5@psu.edu

ABSTRACT

Early fault detection is the primary goal of condition-based maintenance (CBM); to identify an impending fault before failure occurs and provide the necessary maintenance in a timely manner. Machining tools, such as drill bits, require a significant amount of maintenance during industrial machining operations to ensure that workpiece tolerances are met. Faulty tools tend to machine outside expected tolerances and run the risk of causing permanent damage to the workpiece, resulting in added production costs and unwanted delays. Similarly, ball bearing maintenance is crucial for keeping a machine in acceptable working condition, and has been the primary focus of many CBM studies due to nonlinear bearing degradation.

The orthogonal Hilbert-Huang transform (OHHT) is an improvement to the Hilbert-Huang transform (HHT) that is significantly more computationally efficient compared to other improved HHT algorithms. The adaptive nature of the HHT makes it suitable for analyzing nonlinear and non-stationary phenomena and it returns instantaneous energy and frequency results—an advantage over traditional Fourier analysis. This paper showcases the OHHT's potential as a useful diagnostics tool for analyzing machine induced vibration and motor current signals from ball bearing and drilling datasets. Features from the OHHT were fed into a neural network classifier giving health results consistent with another literature study using the same data. Through transfer leaning, a trained neural network from the ball bearing dataset was used to classify drill bit health from the drilling dataset and gave expected health results.

1. INTRODUCTION

Machine maintenance is a necessary part of manufacturing and operations. Equipment eventually wears down and in order for production to run smoothly and efficiently, equipment needs to be maintained in working and acceptable condition. Therefore, maintenance is a necessity and financial plans must account for it—though not all maintenance is useful, or even needed. For example, a U.S. survey found that 33% of all maintenance costs were unnecessary or were the result of poor maintenance plans; the U.S. industry spent more than $200 billion each year on maintenance, resulting in more than $60 billion wasted on unnecessary maintenance as stated by Mobley (2002). It is likely that overall industrial spending—including maintenance costs—has increased since 2002, which calls for a greater need for appropriate and timely maintenance to reduce the amount on unnecessary expenditure.

Predictive maintenance uses direct (e.g., optical) and/or indirect (e.g., vibration, temperature) measurement techniques to quantifiably determine the condition of a machine component [see Ambhore, Kamble, Chinchanikar, & Wayal (2015), Jantunen (2002), and Jardine, Lin, & Banjevic (2006) for a summary of different techniques]. Ideally, predictive maintenance plans allow a given component to be operational until the end of its remaining useful life (RUL); giving notice near the end of the RUL to provide sufficient time to schedule the required maintenance. Different algorithms have been used across the literature to best optimize the ability for a predictive maintenance plan to be effective and has been an on-going area of research.

The Hilbert-Huang transform (HHT) is a signal processing technique whose adaptive nature makes it ideal for analyzing nonlinear and non-stationary phenomena according to Huang, Shen, Long, Wu, Shih, Zheng, Yen, Tung, and Liu (1998) and Huang and Shen (2014). It decomposes an input signal, $x(t)$, through a process called the empirical mode decomposition (EMD), into multiple intrinsic mode functions (IMFs) and a residual signal. Then, it takes the Hilbert transform of each IMF to get its corresponding instantaneous energy density, $E_j(t)$, and instantaneous frequency, $f_j(t)$, where the subscript j corresponds to the jth IMF. Putting all $E_j(t)$ and $f_j(t)$ into a 3-D energy-frequency-time
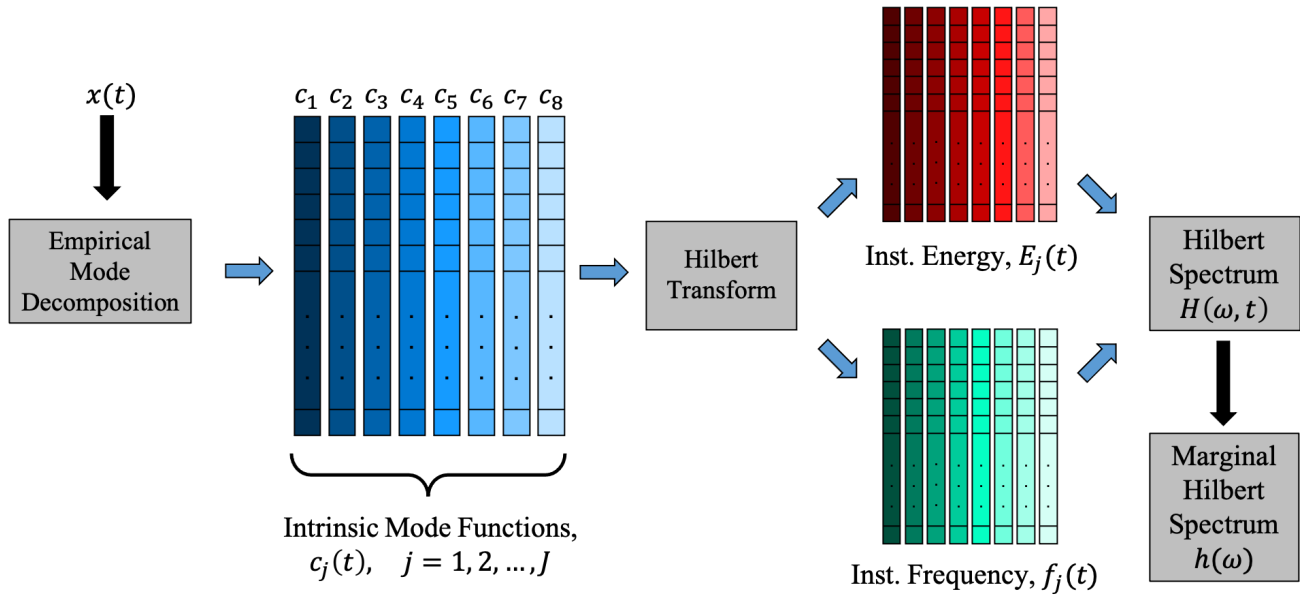
Figure 1. Block diagram of the Hilbert-Huang transform with $x(t)$ having eight intrinsic mode functions (i.e., $J = 8$).

representation is known as the Hilbert spectrum. The Hilbert spectrum can be further condensed into a 2-D energy-frequency representation known as the marginal Hilbert spectrum (MHS). The Hilbert spectrum and marginal Hilbert spectrum are analogous to the spectrogram and power spectral density (PSD) representations respectively, but with the advantage of returning instantaneous frequency and energy results. A summary of the HHT algorithm is shown in the block diagram shown in Figure 1.

The HHT has been used in a number of different applications such as water wave analysis by Huang, Shen, and Long (1999), structural health monitoring by Chen, Zhao, and Li (2014), roller bearing faults by Zheng (2019) and Peng, Peter, and Chu (2005), seismology by Bowman and Lees (2013) and Huang, Lou, Chen, and Wang (2018), electrocardiogram and electroencephalogram analysis by Anuragi and Sisodia (2020) and Yan and Lu (2014), and even flight path characteristics by Mokhtari, Sabzehparvar, and Imani (2020).

Machining often generates nonlinear and non-stationary phenomena according to Dimla Sr and Lister (2000) and Al-Sulaiman, Baseer and Sheikh (2005), so the HHT is expected to be an appropriate method for CBM. The earliest application of the HHT for tool condition monitoring—to the author's knowledge—was proposed by Leisk, Hsu, and Huang (2002), and though the milling results from the computer numeric controller (CNC) machine were preliminary, they anticipated that the HHT would be a very useful tool for future analyses. Since then, the HHT has been used in tool condition monitoring applications such as cutter tool faults by Kalvoda and Hwang (2010), drilling conditions through metal by Wolszczak, Litak, and Dziuba (2018), and using spindle motor current to determine flank wear by Shen, Gui, Chen, Lin, Liu, and Liu (2020) to name a few.

In this paper, the orthogonal Hilbert-Huang transform (OHHT) algorithm presented by Huang et al. (2018) is used to analyze two datasets corresponding to different drilling and ball bearing run-to-failure experiments. The drilling dataset consists of spindle vibration and motor current signals measured by the author using a CNC machine to peck drill holes into a 12"x12"x1" steel plate with the presence of coolant. Unlike other accelerated wear tests that forego using coolant, the purpose of this experiment was to imitate normal cutting conditions while drilling, minimizing the wear induced by heat, to get data that may better represent actual vibration and motor current data measured in an industrial setting. The caveat to this dataset being that it is representative of a single set of drilling parameters which is certainly not exhaustive from a CBM perspective. However, the data was collected every other hole drilled until the drill bit broke while drilling the 817th hole. Each single measurement consisting of 17 unique, extractable signals (one for each peck), so the life of the drill bit is very easy to track with this dataset.

The ball bearing dataset was obtained from the NASA Ames prognostics data repository contributed by Lee, Qiu, Yu, Lin, & Rexnord Technical Services (2007). The ball bearing dataset was analyzed previously by Ali, Fnaiech, Saidi, Chebel-Morello, and Fnaiech (2015) using the EMD technique previously mentioned along with an artificial neural network (ANN) to identify early fault detection. Since the OHHT is just a continuation of the EMD technique, analyzing this dataset using the OHHT should allow for a direct comparison with the results by Ali et al. (2015) to again determine if the OHHT can successfully be used for diagnostics.
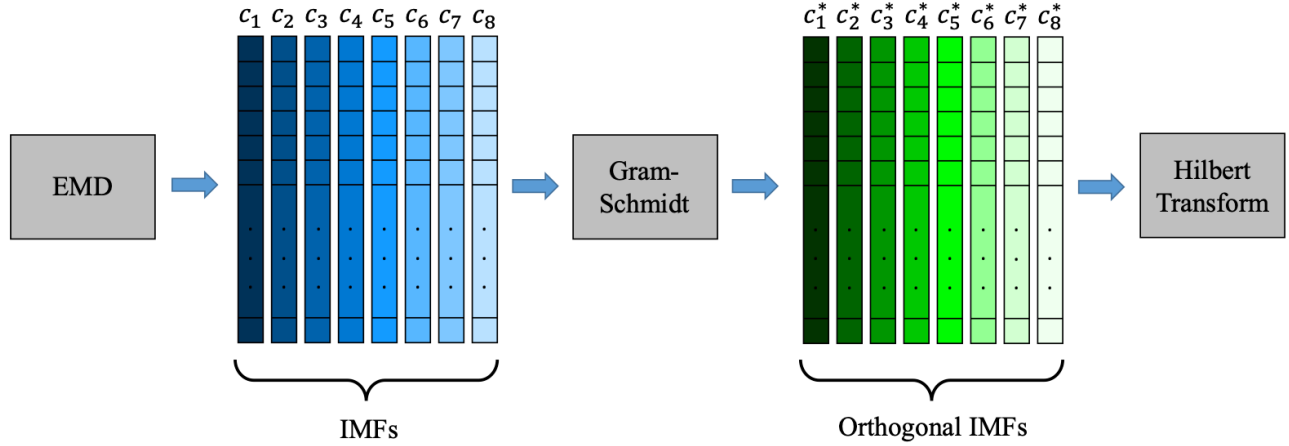
Figure 2. Block diagram for the orthogonal Hilbert-Huang transform with eight example IMFs. After the orthogonal IMFs are calculated, the sequential steps are the same as that of the traditional HHT algorithm (see Figure 1)

Section 2 briefly summarizes how the HHT is used to form the Hilbert spectrum and marginal Hilbert spectrum to define the condition indicator used throughout this work. A brief description of the OHHT and how it improves upon the HHT is also included. More detailed information about the HHT and OHHT can be found in Huang et al. (1998) and Huang et al. (2018) respectively. Section 3 provides information about the individual datasets used in this work. Section 4 presents the OHHT results for each respective dataset, including how the calculated OHHT condition indicators were used with an ANN for health predictions. Lastly, Section 5 presents the conclusions made regarding the use of the OHHT and the ANN for each dataset.

2. THE ORTHOGONAL HILBERT-HUANG TRANSFORM

2.1. The Hilbert-Huang Transform

The Hilbert-Huang transform (HHT) uses a process known as the empirical mode decomposition (EMD) to decompose an input signal, $x(t)$, into multiple intrinsic mode functions (IMFs) suited—ideally—for the Hilbert transform. The jth instantaneous energy densities, $E_j(t)$ and instantaneous frequencies, $f_j(t)$, are obtained for each individual IMF using the Hilbert transform (see Figure 1). The Hilbert spectrum for the jth IMF is then defined as

$$H_j(\omega, t) = \begin{cases} E_j(t), & \omega = 2\pi f_j(t) \\ 0, & \omega \neq 2\pi f_j(t) \end{cases},\qquad (1)$$

and the complete Hilbert spectrum is defined as the summation of all the Hilbert spectra corresponding to each IMF, where J is the total number of IMFs, namely

$$H(\omega, t) = \sum_{j=1}^{J} H_j(\omega, t).\qquad (2)$$

The definitions of Eqs. (1) and (2) are a sparse matrix representation of the Hilbert spectrum and are formal definitions of $H(\omega, t)$ [as found in Wikipedia (2020)], whereas many papers addressing the HHT simply infer the definition of $H(\omega, t)$ and use the same, if not identical, explanations set forth by Huang et al. (1998).

The marginal Hilbert spectrum (MHS) is defined as

$$h(\omega) = \int_0^T H(\omega, t)\, dt,\qquad (3)$$

where T is the duration of $x(t)$, and thus sums the instantaneous energy content over time into single frequency bins. The interpretation of the MHS, however, varies slightly from that of its Fourier 'cousin', the PSD. Frequency peaks in $h(\omega)$ do correspond to energy at a given frequency, but more so probabilistically. It is normal to see frequency peaks with a Gaussian-like shape in the MHS, where a narrower peak indicates a greater likelihood of finding a given frequency in the Hilbert spectrum at a given time.

2.2. Hilbert Spectrum Condition Indicators

Shen et al. (2020) correlated flank wear to the maximum value of the marginal Hilbert spectrum using motor current signals. Their indicator is defined in this work as

$$\eta_1 = \max\{h(\omega)\},\qquad (4)$$

2.3. The Orthogonal Hilbert-Huang Transform

Ideally, EMD produces IMFs that are orthogonal to each other, such that the energy between two orthogonal signals [e.g., $p(t)$ and $q(t)$] will be zero, i.e.,

$$E = \int_0^T p(t)q(t)\, dt = 0.\qquad (5)$$

However, IMFs produced from measured data tend not to be orthogonal, which can result in significant energy loss in the IMFs. Huang et al. (2018) developed an improved[1] HHT algorithm called the orthogonal Hilbert-Huang transform (OHHT) which uses a Gram-Schmidt method to generate orthogonal IMFs (see Figure 2). These orthogonal IMFs significantly reduce the amount of energy leakage compared to the traditional HHT algorithm, and Huang et al. (2018) determined that these IMFs can significantly reduce the energy leaked to less than 1%. Their 'forward' method for sorting the IMFs prior to using the Gram-Schmidt method was used in this work. Refer to Huang et al. (2018) for additional information about implementing the Gram-Schmidt method to orthogonalize the IMFs and the differences between their IMF sorting methods.

One of the OHHT's primary benefits is its computational efficiency compared to other improved HHT algorithms. The HHT, generally speaking, is not a very quick signal analysis tool—especially when computing long signals with high sampling rates—and many of the improved HHT algorithms add a significantly longer runtime due to additive white-noise ensemble averaging involving hundreds of copies of $x(t)$ [see Wu & Huang (2009)]. The Gram-Schmidt method is computationally efficient by itself, so the OHHT algorithm runs only marginally slower than that of the traditional HHT algorithm, with the added benefit of having orthogonal IMFs producing minimal energy leakage.

3. MACHINING AND BALL BEARING DATASETS

The OHHT was used on different types of machining datasets experiencing some form of machine failure. A drilling dataset was used to monitor flank wear indirectly on a drill bit during machining operations. An additional bearing dataset was also analyzed for identifying known bearing faults included with the dataset's documentation. A description of each dataset and how they were obtained is described in the following sections. The raw data from each dataset was collected without using any sort of CBM algorithms in real-time.

3.1. NASA IMS Bearing Dataset

The degradation of bearings is considered a nonlinear process, which can be seen from the NASA IMS bearing dataset [Lee, et al. (2007)]. Early stage detection should be indicative that the bearing is beginning to fail and that maintenance should be scheduled. However, degradation can occur suddenly and rapidly, which can make it difficult to perform the necessary maintenance in time to remove the faulty bearing and replace it with a new bearing.

Three run-to-failure experiments were conducted by applying an equal radial load of 6000 lbs. to four Rexnord ZA-2115 double row ball bearings installed along a shaft. The shaft was rotated at a constant 2000 rpm using an AC motor with rub belts and the bearings were all force lubricated for each experiment. Each of the three experiments concluded after a sufficient amount of degraded material made its way through the lubrication system and became stuck to a magnetic switch that powered off the machine. Vibration measurements were collected using PCB 353B33 High Sensitivity Quartz ICP accelerometers mounted on each bearing [see Figure 16 in Qiu, Lee, Lin, & Yu (2006) for installation locations]. A one second block of vibration data was collected approximately every 10 minutes[2] sampled at $f_s = 20$ kHz.

Though the same radial load was applied to each bearing, only certain bearings had significant amounts of degradation. The defects identified were roller element faults, outer race faults, and inner race faults. The bearings that did end up failing did not all experience the same type of degradation; even the bearings that did have the same type of degradation across different run-to-failure experiments did not all fail after the same number of rotations.

3.2. Drilling Dataset

A Haas VF-4 CNC machine was used to peck-drill holes into a 12"x12"x1" square plate of A36 low carbon steel with the presence of lubricant/coolant. A brand new solid carbide 1/4"diameter drill bit was used to repeatedly peck drill holes into the plate until the bit broke. The holes were spot-drilled in a 29x29 grid pattern prior to the actual run-to-failure experiment, being spaced 3/8" from an adjacent hole, resulting in 841 potentially drilled holes, but during the actual experiment, the new drill bit broke—shattered into multiple pieces—while drilling the 817th hole. The CNC spindle shaft speed and feed rate remained constant for each drilled hole, which were set to 1600 rpm and 6.5 in/min respectively.

A PCB Piezotronics 356A03 tri-axial accelerometer was magnetically mounted to the CNC stationary spindle housing with the x-axis accelerometer is in the direction most sensitive to shear and reaction torque, the y-axis normal to the spindle housing, and the z-axis in the same direction of axial thrust (i.e., downward, see Figure 3). The z-axis is the most sensitive to drilling vibration as it picks up on the thrust force used to drill into the plate, and the x-axis is the least sensitive since the magnetic mount makes the accelerometer not ideal for measuring reaction torque. Additionally, LEM HAL 50-S electric current sensors were installed on each of

---

[1] **Note**: A literature search on "Improved Hilbert-Huang transform" will yield multiple, different HHT algorithms despite many of them being called the same name. A summary of some of the different improvements made to the HHT over the years can be found in Colominas, Schlotthauer, & Torres (2014) and Furlong (2021).

---

[2] The dates and times for a given vibration measurement are included in the file name of each data measurement. Examination of these times shows several days between some consecutive measurements, primarily from the first run-to-failure experiment, so the data was not continuously measured every 10 minutes as stated previously. The results in this paper are presented as if the data was collected every 10 minutes to allow for direct comparison with the results by Ali et al. (2015).

Figure 3. Picture of the magnetically mounted tri-axial accelerometer (circled in red) on the CNC spindle housing with the direction of its positive y and z-axes.

the three phases of the spindle and feed motors to collect both vibration and motor current data from the drilling operation. The wires for each phase leading to said motors were wrapped around an individual current sensor to increase the signal-to-noise ratio of each sensor, with the number of wrappings based on the expected output motor current (five times for the feed motor and three times for the spindle motor). For brevity, only the z-axis vibration and spindle motor current results are shown in this paper despite some promising behaviors observed in the other three sensors.

The vibration and motor current data was collected using a National Instruments (NI) PXI-1031 DC chassis with an NI PXI-8183 embedded controller and NI 4472B data acquisition cards sampled at $f_s = 25$ kHz in 25 second blocks to measure all the pecks required to drill a single hole. The data was collected every other hole drilled resulting in a total number of 409 unique records in the dataset. Each hole consisted of 17 pecks—including the entry and exit pecks which did not remove equal amounts of material as the other 15 pecks—which were extracted individually from each record, resulting in a total of 6953 unique signals for each sensor.

The vibration and motor current data were filtered in post-processing prior to calculating the OHHT, with filter parameters varying by sensor. The z-axis accelerometer used a 64th order FIR band pass filter with cutoff frequencies of 2 to 6 kHz and the spindle motor current LEM sensors used a 512th order FIR low-pass filter with a cutoff frequency of 200 Hz. The filter coefficients and filtering were performed in MATLAB using the *fir1()* and *filtfilt()* commands

respectively. The window used for the *fir1()* command was the default Hamming window for all sensors. Additionally, the spindle motor current was analyzed by combining the three phase signals into a single signal using the equation

$$I_{rms} = \sqrt{\frac{1}{3}(I_u^2 + I_v^2 + I_w^2)}, \qquad (16)$$

where I_u, I_v, and I_w are the current measured from the three respective phases. This process is commonly used for converting an AC current to an equivalent DC current according to Sevilla-Camacho, Herrera-Ruiz, Robles-Ocampo, & Jáuregui-Correa (2011). However, unlike a true DC signal, I_{rms} in this case preserves its frequency content, making frequency analysis using the OHHT possible.

4. RESULTS AND DISCUSSION

4.1. NASA IMS Bearing Dataset Results

Ali et al. (2015) conducted a study using the EMD technique with an artificial neural-network (ANN) to analyze this dataset to determine how well the ANN could identify early stage fault detection. Their ANN results were able to predict up to seven different classifications of wear (i.e., healthy, degraded roller/inner race/outer race, and failure roller/inner race/outer race) from the time series data using the EMD and statistical features. Said classification results were used to calculate a health index (HI) metric to identify early bearing degradation, which was simply calculated by adding a value of one to HI whenever a 'not healthy' result was predicted. The defined "early stage" degradation [see Figures 11–13 in Ali et al. (2015)] begins when the HI exceeds a value of 0, but "severe degradation" is not explicitly defined and appears to vary from bearing to bearing based solely on the value of HI. See Table 1 for the degradation results of Ali et al. (2015).

Bearing Info.	Fault Type	Early Stage [10 min]	Severe Degradation [10 min]
Test 1, Bearing 4	Roller Element	1560	1953
Test 1, Bearing 3	Inner Race	1561	1854
Test 2, Bearing 1	Outer Race	553	914
Test 3 Bearing 3	Outer Race	211	N/A

Table 1. Early stage and severe degradation results by Ali et al. (2015) for bearings with known faults.

The OHHT results presented in this paper are directly compared to the results presented by Ali et al. (2015). The OHHT is a continuation of the same EMD technique used by Ali et al. (2015), which makes the comparison appropriate using the same dataset. As such, an ANN patterned after Ali et al. (2015) was used to classify the same classes using input features extracted from the OHHT (see Figure 4). A similar HI will be calculated and will be compared to the HI results by Ali et al. (2015).

The dataset is inherently unlabeled, and Ali et al. (2015) do not specify how they labeled the data for training their ANN. Refer to Table 2 for how the data was classified in this work.

Bearing Info.	Fault Type	Healthy	Degraded	Failure
Test 1, Bearing 4	Roller Element	1:1200	1700:1749	2106:2155
Test 1, Bearing 3	Inner Race	1:1200	2000:2049	2106:2155
Test 2, Bearing 1	Outer Race	1:500	850:899	934:983

Table 2. Files labeled for training the ANN. Total of 2900 healthy files and 50 files for all other classes.

4.1.1. OHHT Feature Extraction

The MHS was calculated for each vibration measurement using a frequency resolution of 10 Hz and was measured in dB re: $1 \mu g$. A moving average filter with a window size of 20 samples was applied to $h(\omega)$ to smooth out the frequency results, then the first six local maxima peaks—similar to η_1—having a width of 3 samples separated by at least 20 samples, were extracted. The frequency locations of each local maxima were also extracted resulting in a total of 12 OHHT input features. The features are all standardized prior to passing them into the ANN. On average, it takes approximately 0.33 s to calculate all 12 features from a single vibration signal for this dataset.
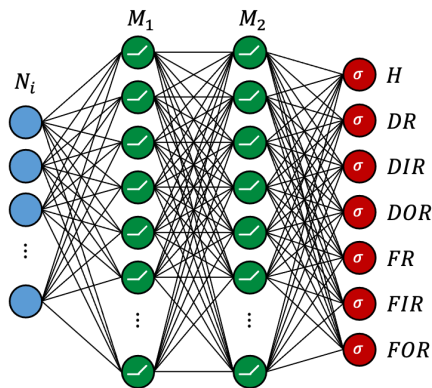

Figure 4. Diagram of the ANN model used in this work for bearing health classification. The number of nodes for the input and hidden layers are N_i, M_1, and M_2 respectively.
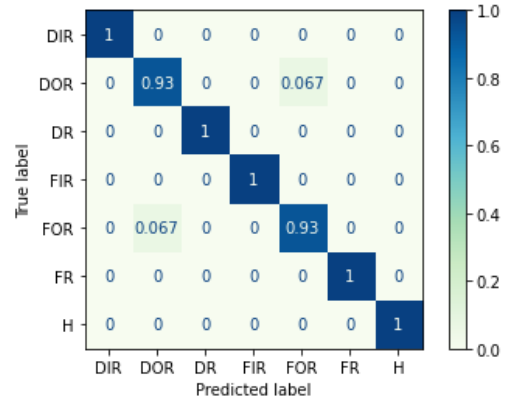

Figure 5. Confusion matrix accuracy results for the trained bearing health classifier ANN.

4.1.2. ANN Parameters and Training

Ali et al. (2015) used a fully connected ANN having an input layer with 18 nodes, two hidden layers with 20 and 18 nodes respectively, and an output layer with only four nodes. Each layer had a "hyperbolic tangent sigmoid" activation function. The 18 input features include ten statistical features and the energy ratio of eight IMFs to the total IMF energy [see section 3.2 in Ali et al. (2015) for additional information].

The ANN used in this work was built using TensorFlow and similarly has four layers (see Figure 4): the input layer has 12 nodes, the first and second hidden layers have 118 and 122 nodes respectively, and the output layer has seven nodes corresponding to each output class. The number of nodes for the hidden layers were hypertuned using GridSearchCV starting with a range of 10 to 150 nodes per layer at intervals of 20. The search grid was refined at varying intervals using previous 'best parameters' until arriving at 118 and 122 nodes. The ReLu activation function was used for all layers except the output layer, which used the "softmax" activation function. The model was compiled using the Adam optimizer, the categorical cross-entropy loss function, and accuracy as an additional metric.

The labeled data (see Table 2) was shuffled, stratified, and split into training and test data using a 70-30 split. The model was then trained with a batch size of 16 and 150 epochs. The model achieved a total accuracy of 99.79% with all individual classes achieving at least a 93% accuracy (see Figure 5).

4.1.3. ANN Results

The health index used on the ANN results is similar to that of Ali et al. (2015) with a few minor adjustments. To mitigate potential false alarms, HI will not begin incrementing until there are a consecutive number of 'not healthy' classifications—in this work, that number is three. Upon activation, any degradation predictions will increase HI by +1
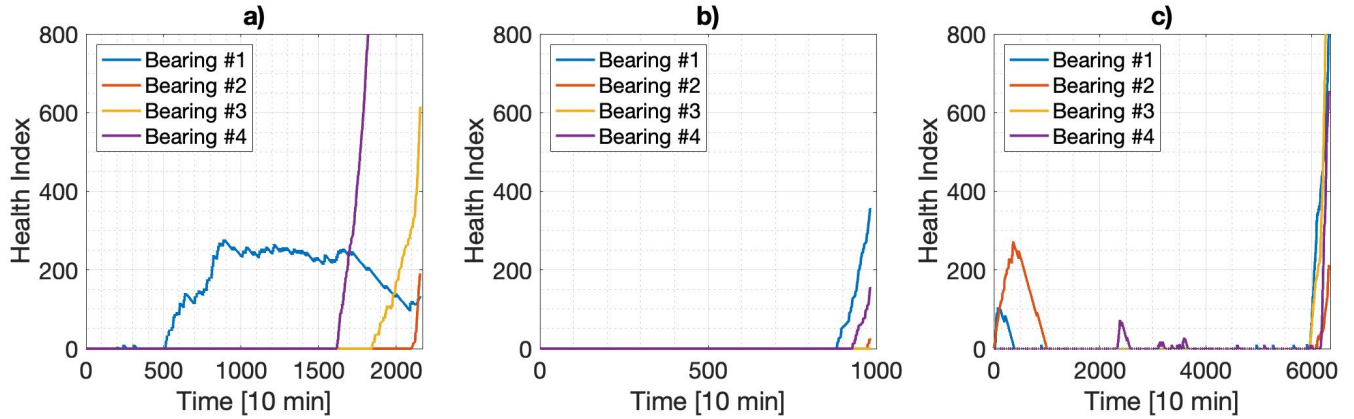
Figure 4. Health index results from the trained ANN using MHS input features extracted from the IMS bearing vibration data corresponding to a) test #1, b) test #2, and c) test #3.

and any failure predictions will increase HI by +10, thereby giving greater weight to failure predictions. Should the ANN make any healthy prediction after activation, HI will change by −0.5, allowing HI to forget potential misclassifications related to possible equipment start-up transients, "break-in" periods, etc. that can occur. The larger this weight is, the faster HI will forget past classifications; preventing HI being biased closer to failure by past potential misclassifications.

Figure 4 shows the HI results for all the bearing vibration data. The bearings with known faults (see Table 1) are clearly identified, such that setting an example HI threshold of 300 identifies all these bearings as needing replacement. It even identifies other bearings [e.g., Figure 4b), bearing 4] that started exhibiting wear that may not have been previously identified or reported, which is consistent with the conclusions made by Ali et al. (2015) and their model. While the early stage degradation points (i.e., the first time HI $\neq$ 0) in Figure 4 may not all line up with those identified in Table 1, the modified HI makes for a more generalizable metric which clearly identifies early stage degradation and severe degradation—assuming pre-defined degradation thresholds for HI.

4.2. Drilling Dataset Results

4.2.1. Hole Tolerance Measurements

Using go/no-go probes, the tolerance of each hole was measured showing that the first 670 holes drilled consistently stayed within a tolerance < 0.2510". After the 671st hole, the hole tolerance quickly (within 8 holes) exceeds 0.2546" until around the 700th hole, where the hole tolerances become more inconsistent; few holes actually measure < 0.2510", but most exceed values of 0.2520" or 0.2546".

4.2.2. Vibration and Motor Current Results

Figure 5 shows results performing k-means clustering using three clusters on spindle motor current (MC) and z-axis accelerometer data. The RMS for each peck signal was

calculated for both the vibration and motor current data and are plotted as black dots on the x and y-axes respectively in Figure 5a). The value of η_1 was calculated for the vibration data and replaced the x-axis in Figure 5b) which appears to have a power relationship in the form $f(x) = ax^b$. The three cluster regions calculated could approximate the condition of the drill bit and have been labeled as 'healthy', 'worn', or 'failure' and are colored green, yellow, and red respectively.

The light green and orange dots correspond to the entry and exit pecks respectively and are marked since they appear to have their own clusters in Figure 5a). This is not entirely surprising since they remove different amounts of material than the other pecks. The entry and exit pecks appear to follow the behavior of the other pecks in Figure 5b), yet when viewed over time, their behaviors invert (i.e., the entry peck started with greater energy and ended with less energy than
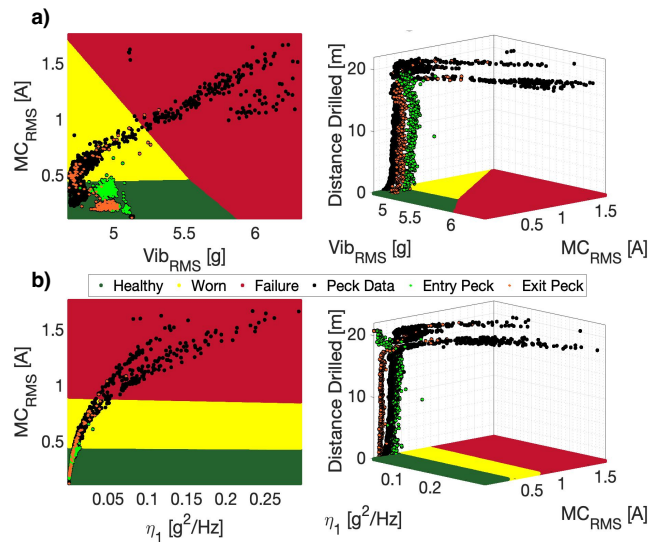

Figure 5. Comparison of k-means clustering results using the RMS spindle motor current and the a) vibration RMS and b) η_1 from the vibration. The plots on the right contain the same information plotted over time.

the exit peck) and cross at around the 700th hole: the assumed point of initial failure. Additional research could be done to evaluate the ratio of the entry and exit peck energy as a condition indicator for monitoring wear.

The data in Figure 5 shows the vibration and motor current results staying in the healthy region until around 17.25 m of cumulative drilling distance, where it begins to regularly transition to the worn region—around the 680th hole. The data regularly transitions to the failure region at 17.78 m, which corresponds to the 700th hole. The data shortly returns primarily to the worn region, then returns to the failure region around 20.5 m (around the 810th hole) until the drill bit breaks. These health regions are promising in that once the data begins to enter the failure region, the data regularly stays in either the worn or failure regions. These results also appear consistent with the hole tolerance results.

4.2.3. ANN Transfer Learning Results

Given the similarity in tasks between the bearing and drilling datasets using the OHHT, the trained ANN used for the bearing dataset was modified through transfer learning to classify the drilling dataset. The following considerations are addressed in order to perform transfer learning: 1) The number of OHHT features differ between the bearing and drilling datasets, thus affecting the number of input features needed for the transferred model. 2) The drilling dataset can be classified using three health classes (see Figure 7) similar to the seven output classes used in the trained ANN. Therefore, the weights connecting to/from the hidden layers
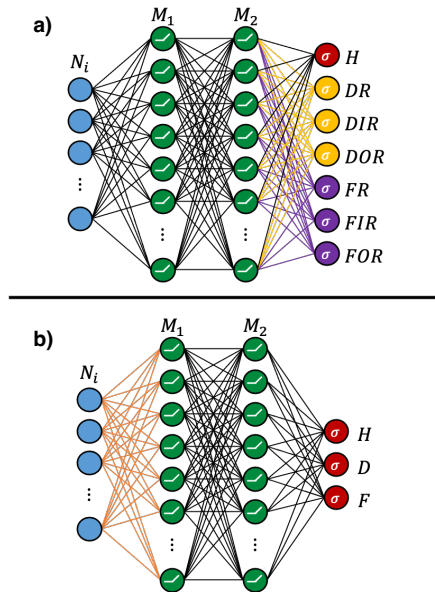

Figure 8. Steps for transfer learning using the trained ANN. a) Averaging the output weights and nodes by class (denoted by color). b) Training only the weights from the input layer to the first hidden layer (the orange lines).
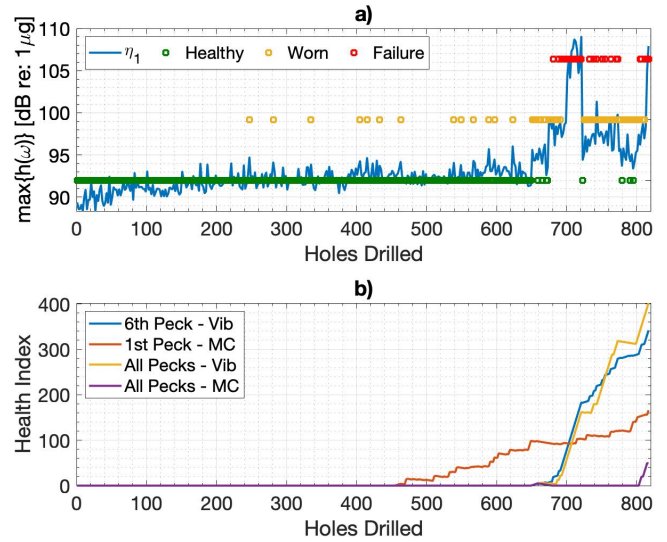

Figure 9. Drilling dataset results: a) Values of η_1 for the z-axis vibration data and the ANN predictions using the single peck model. b) Health index results for single peck and single hole models for the vibration and motor current data.

are affected and need retrained. The weights and nodes for the hidden layers, however, remain untouched (i.e., frozen).

The three output classes for the new model—'healthy', 'degradation', and 'failure'—are evaluated using the weights connected to the output layer and node values of similar classes from the trained ANN [see Figure 8a]. The three sets of weights and nodes for a given class (e.g., 'failure') from the trained ANN are averaged to form one set of weights and node per class. This ensures that the only parameters in the transferred model that need training are the weights connecting the input layer to the first hidden layer [see Figure 8b]. These weights are then trained—after freezing all other parameters—for 300 epochs using sensor data from the first 20 healthy holes and four holes each from the worn and failure regions found in Figure 7.

The number of input features varied based on the sensor data analyzed and if the ANN should make a prediction for a single peck measurement or for a single-hole measurement (i.e., all 17 pecks). The z-axis vibration data has a single prominent peak in the MHS, so the input features are the peak value, η_1, and its frequency location for each peck (i.e., two features per peck). The spindle motor current data has four prominent peaks in the MHS so it has eight input features per peck (see Table 3 for a summary of input features per model). Single peck and single hole models were tested for both the vibration and motor current data and HI was calculated or each model as was done previously with the bearing ANN.

The results of the modified ANN shown in Figure 9 appear to favor the vibration dataset over the spindle motor current dataset. The HI results for the vibration data are nearly similar for both the single peck and single hole models and the ANN predictions are consistent with the k-means clustering and

Model	Vibration	Motor Current
Single Peck	2	8
Single Hole	34	136

Table 3. Number of input features by sensor for each model.

hole tolerance results. The motor current models either predict drill bit degradation significantly early in the case of the single peck model, or just before the drill bit broke in the case of the single hole model. Perhaps this means that some of the motor current data's prominent peaks in the MHS do not actually contribute to predicting the drill bit's health. This could explain why adding more potentially extraneous features inhibited the single hole model's performance, while using fewer of these features allowed the single peck model to perform better than the single hole model. Additional research could be done to verify which peak(s) improve classification results, and if there is a correlation between said frequencies and the physical system parameters.

5. CONCLUSION

The HHT is relatively new in its application to the field of CBM, but it offers many strengths that make it a valuable signal processing method. It is suitable for analyzing nonlinear and non-stationary phenomena, such as machining, with the added benefit of including time-frequency information in the form of either the Hilbert spectrum or the MHS. The OHHT is an improvement to the HHT in terms of energy leakage and computation speed (compared to other improved HHT algorithms) and is relatively simple to implement and understand.

The proposed condition indicator in this paper utilizes the OHHT to pull information from the frequency domain in order to classify the health of a given machine component. A general behavior observed across the datasets is that an increasing value in η_1 results in greater wear and degradation for both vibration and motor current signals. An ANN for classifying the health of a given part was initially trained on the bearing dataset with success consistent with similar analyses in the literature. The same ANN was modified through transfer learning for use on the drilling dataset and showed similar success in predicting tool wear. These results strengthen the claim that the OHHT is applicable for general CBM applications, despite the fact these datasets represent a small sample of machining conditions, components, or workpiece materials.

REFERENCES

Al-Sulaiman, F. A., Baseer, M. A., & Sheikh, A. K. (2005). Use of electrical power for online monitoring of tool condition. *Journal of Materials Processing Technology*, *166*(3), 364-371.

Ali, J. B., Fnaiech, N., Saidi, L., Chebel-Morello, B., & Fnaiech, F. (2015). Application of empirical mode decomposition and artificial neural network for automatic bearing fault diagnosis based on vibration signals. *Applied Acoustics*, *89*, 16-27.

Ambhore, N., Kamble, D., Chinchanikar, S., & Wayal, V. (2015). Tool condition monitoring system: A review. *Materials Today: Proceedings*, *2*(4-5), 3419-3428.

Anuragi, A., & Sisodia, D. S. (2020). Empirical wavelet transform based automated alcoholism detecting using EEG signal features. *Biomedical Signal Processing and Control*, *57*, 101777.

Bowman, D. C., & Lees, J. M. (2013). The Hilbert–Huang transform: A high resolution spectral method for nonlinear and nonstationary time series. *Seismological Research Letters*, *84*(6), 1074-1080.

Chen, B., Zhao, S. L., & Li, P. Y. (2014). Application of Hilbert-Huang transform in structural health monitoring: a state-of-the-art review. *Mathematical Problems in Engineering*, *2014*.

Colominas, M. A., Schlotthauer, G., & Torres, M. E. (2014). Improved complete ensemble EMD: A suitable tool for biomedical signal processing. *Biomedical Signal Processing and Control*, *14*, 19-29.

Dimla Sr, D. E., & Lister, P. M. (2000). On-line metal cutting tool condition monitoring.: I: force and vibration analyses. *International Journal of Machine Tools and Manufacture*, *40*(5), 739-768.

Furlong, T. S., (2021). *Tool Condition Monitoring Using the Hilbert-Huang Transform: An Application to Vibration and Motor Current Signals*. Master's thesis. The Pennsylvania State University, State College, PA 16801, United States. https://etda.libraries.psu.edu/catalog/18555tsf44

Huang, N. E., & Shen S. S. P. (2014). *Hilbert-Huang transform and its applications* (Vol. 16). World Scientific.

Huang, N. E., Shen, Z., & Long, S. R. (1999). A new view of nonlinear water waves: the Hilbert spectrum. *Annual review of fluid mechanics*, *31*(1), 417-457.

Huang, N. E., Shen, Z., Long, S. R., Wu, M. C., Shih, H. H., Zheng, Q., Yen, N. C., Tung, C. C., & Liu, H. H. (1998). The empirical mode decomposition and the Hilbert spectrum for nonlinear and non-stationary time series analysis. *Proceedings of the Royal Society of*

London. *Series A: mathematical, physical and engineering sciences*, *454*(1971), 903-995.

Huang, T. L., Lou, M. L., Chen, H. P., & Wang, N. B. (2018). An orthogonal Hilbert-Huang transform and its application in the spectral representation of earthquake accelerograms. *Soil Dynamics and Earthquake Engineering*, *104*, 378-389.

Jantunen, E. (2002). A summary of methods applied to tool condition monitoring in drilling. *International Journal of Machine Tools and Manufacture*, *42*(9), 997-1010.

Jardine, A. K., Lin, D., & Banjevic, D. (2006). A review on machinery diagnostics and prognostics implementing condition-based maintenance. *Mechanical systems and signal processing*, *20*(7), 1483-1510.

Kalvoda, T., & Hwang, Y. R. (2010). A cutter tool monitoring in machining process using Hilbert–Huang transform. *International Journal of Machine Tools and Manufacture*, *50*(5), 495-501.

Lee, J., Qiu, H., Yu, G., Lin, J., & Rexnord Technical Services (2007). IMS, University of Cincinnati. "Bearing Data Set", NASA Ames Prognostics Data Repository [http://ti.arc.nasa.gov/project/prognostic-data-repository], NASA Ames Research Center, Moffett Field, CA.

Leisk, G. G., Hsu, N. N., & Huang, N. E. (2002). Application of the Hilbert-Huang transform to machine tool condition/health monitoring. In *AIP Conference Proceedings*(Vol. 615, No. 1, pp. 1711-1718). American Institute of Physics.

Mobley, R. K. (2002). *An introduction to predictive maintenance*. Elsevier.

Mokhtari, S. A., Sabzehparvar, M., & Imani, K. (2020). Nonlinear Flight Mode Identification by Applying Modified Ensemble Empirical Mode Decomposition and Hilbert–Huang Transformation. *International Journal of Aeronautical and Space Sciences*, *21*(4), 1161-1173.

Qiu, H., Lee, J., Lin, J., & Yu, G. (2006). Wavelet filter-based weak signature detection method and its application on rolling element bearing prognostics. *Journal of sound and vibration*, *289*(4-5), 1066-1090.

Peng, Z. K., Peter, W. T., & Chu, F. L. (2005). A comparison study of improved Hilbert–Huang transform and wavelet transform: application to fault diagnosis for rolling bearing. *Mechanical systems and signal processing*, *19*(5), 974-988.

Sevilla-Camacho, P. Y., Herrera-Ruiz, G., Robles-Ocampo, J. B., & Jáuregui-Correa, J. C. (2011). Tool breakage detection in CNC high-speed milling based in feed-motor current signals. *The International Journal of Advanced Manufacturing Technology*, *53*(9-12), 1141-1148.

Shen, B., Gui, Y., Chen, B., Lin, Z., Liu, Q., & Liu, Q. (2020). Application of spindle power signals in tool condition monitoring based on HHT algorithm. *The International Journal of Advanced Manufacturing Technology*, *106*(3), 1385-1395.

Wikipedia. (2020, March 20). *Hilbert spectrum.* Retrieved June 6, 2020, from https://en.wikipedia.org/wiki/Hilbert_spectrum.

Wolszczak, P., Litak, G., & Dziuba, M. (2018). Monitoring of drilling conditions using the Hilbert-Huang transformation. In *Matec web of Conferences* (Vol. 148, p. 16003). EDP Sciences.

Wu, Z., & Huang, N. E. (2009). Ensemble empirical mode decomposition: a noise-assisted data analysis method. *Advances in adaptive data analysis*, *1*(01), 1-41.

Yan, J., & Lu, L. (2014). Improved Hilbert–Huang transform based weak signal detection methodology and its application on incipient fault diagnosis and ECG signal analysis. *Signal Processing*, *98*, 74-87.

Zheng, Y. (2019). Predicting remaining useful life based on Hilbert–Huang entropy with degradation model. *Journal of Electrical and Computer Engineering*, *2019*.

BIOGRAPHIES

Trent S. Furlong was born and raised in the state of Utah, where he earned his Bachelor's degree in Applied Physics from Brigham Young University, Provo, UT, United States in 2018. He then went on to earn his Master's degree in Acoustics from The Pennsylvania State University, State College, PA, United States in 2021. He is presently working on his Doctorate in Acoustics at The Pennsylvania State University, State College, PA, United States. His current research interests include signal processing and vibration analysis. He is a member of the Acoustical Society of America and the Penn State Center for Acoustics and Vibration.

Dr. Karl M. Reichard is an Associate Research Professor with the Applied Research Laboratory and the Graduate Program in Acoustics at Penn State University. He is also the head of the Applied Research Laboratory's Embedded Monitoring and Control Systems Department. The department conducts research and develops systems for the monitoring, diagnosis and prediction of health and status in mechanical and electrical systems. Dr. Reichard received the Ph.D., M.S. and B.S. degrees in Electrical Engineering from the Virginia Polytechnic Institute and State University (Virginia Tech). He is a member of the Board of Directors of the Prognostics and Health Management Society, and a member of the IEEE and the Acoustical Society of America.